Progress In Electromagnetics Research M, Vol. 97, 35–44, 2020

Photonic-Crystal Substrates for Harmonic Suppression in Multi-Band Smart Devices

Omar Siddiqui, Raghied Atta, Muhammad Amin, and Hattan Abutarboush*

Abstract—We propose photonic crystal substrates that support microstrip structures to mitigate the problem of spurious harmonics in microwave devices. The wave propagation in microwave transmission lines can be controlled by employing substrates that have modulated dielectric constant such that there exist forbidden spectral regions, which are known as *bandgaps* in the photonic crystal terminology. With proper selection of crystalline geometry, these bandgaps can be designed to suppress the spurious harmonics. To show the existence of bandgaps in microstrip structures, we present Bloch analysis with a bi-layered photonic crystal configuration of high and low permittivities. For a practical microstrip structure that incorporates a bi-layered photonic crystal substrate, we show suppression of spurious harmonics via circuit analysis and transmittance measurements. Furthermore, a 2.5 GHz coupled-line filter is designed on a photonic crystal substrate, and 30 dB second harmonic suppression at 5 GHz is experimentally demonstrated. With the current trend multiple device integration on single platform, the photonic crystal substrates can potentially provide the noise suppression and spurious harmonic rejection needed for microwave components occupying close proximity.

1. INTRODUCTION

Late 1980s marked the discovery of artificially manufactured crystal-like structures that interact with electromagnetic waves in a manner similar to the behavior of natural crystals in the presence of electron waves [1–3]. Thereby, the term *photonic crystals* was rightly coined to signify this analogous behavior. Subsequently, Bloch analysis was applied to characterize the well-known phenomena of Bloch waves, forbidden energy gaps, and wave dispersion in the photonic crystals [1, 4]. Since the crystalline lattice behaved as an effective medium in the low frequency regime (where wavelengths are much larger than the unit cells), interesting wave effects such as the bandgaps and backward wave propagation were observed in the higher order spectra [5]. The advent of *metamaterials* at the beginning of the twentieth century can be regarded as a milestone in the field of dispersion engineering. With the advancement in metamaterial research, true artificial bulk media were realized that possessed properties beyond the nature, such as negative index of refraction, sub-wavelength focussing and image resolution. This term 'metamaterial' initially represented the media that possessed negative refractive index in the fundamental Brillouin zone [6, 7]. This term is now used to describe artificial structures characterized by unique dispersive properties, such as the plasmonic [8], chiral [9], and photonic [10, 11] metamaterials. Similar phenomena were also observed in photonic crystals in the higher order optical regimes [12, 13].

Photonic crystals and metamaterial research kindled strong inspiration in the microwave community to exploit dispersion control with these periodic structures leading to novel implementations of conventional microwave applications [14–20]. One of the earlier works suggested the suppression of image currents and surface-waves propagating on an antenna ground plane using a high impedance electromagnetic bandgap (EBG) structure [14]. The EBG structure consisted of hexagonal patches printed on a dielectric substrate and connected to a ground plane through vertical vias (mushroom

Received 12 August 2020, Accepted 9 September 2020, Scheduled 28 September 2020
* Corresponding author: Hattan F. Abutarboush (dr.abutarboush@gmail.com).
The authors are with the College of Engineering, Taibah University, Madinah, Saudi Arabia.

structure). The ground breaking work on high impedance surfaces was followed by plethora of research efforts that exploited the periodic structures (EBGs, photonic crystals, and metamaterials) in all areas of microwave engineering, including antenna design [14, 19, 21–25] phase shifters [22, 23, 26], filters [19, 27] and other frequency selective devices [18, 20, 28, 29]. Most of these periodic structures exploited metallic inclusions contained in a background dielectric, thus resulting in strong dispersion that led to novel devices. However, due to the fact that these strong dispersive effects occur close to resonances, such as in the case of the well-known negative index medium [6], high conductive losses accompanied the interesting underlying phenomenon. Moreover, the use of metallic structures [18] and lumped components [16, 19] increased the complexity of fabrication and the need for a difficult design procedure which may vary from one application to another. More recently, the photonic crystals and periodic structures have been exploited in useful applications in optical spectrum, such as haemoglobin detection in human blood [30], nanometric scale optical devices [31] and high-Q optical sensors [32].

The scope of this paper is limited to the photonic crystals (or EBGs) that support microwave transmission lines and are formed by periodic repetitions of dielectric configurations without the use of metallic inclusions. Throughout this paper, we will refer to these structures as '*photonic crystal substrates*' (*PC-substrates*). Consider two such configurations depicted in Fig. 1. The first substrate is the well-known 2D photonic crystal [4] with cylindrical cavities separated by a periodicity of $d = 1\,\text{cm}$ in a dielectric material (having $\varepsilon = 4$). The second substrate is the bi-layered photonic crystal composed of alternating dielectric layers with relative permittivities 2.3 and 6.15, repeated with a periodicity of 2 cm. A quick periodic analysis using the MBP simulation package [33] gives the band diagram for the two structures (Fig. 1) showing the pass-bands and the bandgaps. The simulation assumes periodic boundary conditions in the three dimensions and electric fields orientated in the z-directions to simulate an environment similar to the microstrip structures. Note that the wavelength remains significantly larger than the unit cell in the lowest passband of propagation (the fundamental band). Hence an effective dielectric constant can be defined, which is useful to design microwave components that work in this regime. The wave propagation in the periodic structures (i.e., the pass and stop band regimes) can be controlled by the proper choice of geometrical parameters like periodicity and other physical dimensions.

The concept of (non-metallic) photonic-crystal based microwave substrates can be found in some of the early research works [34, 35]. Surprisingly, it did not gain much popularity among the microwave community, probably due to the complexity of the underlying manufacturing process. However, with the recent trend of multiple device integration (such as in smart phones), the requirement for space-efficient filters has also increased. At the same time, the recent advancements in fabrication techniques such as the 3D printing, the material patterning and fusion have become a household phenomenon. Therefore, we feel there is a need to have a fresher look on the patterned all-dielectric PC-substrates which have natural filtering abilities and hence are superior than the ordinary substrates in multiband applications. Particularly, in an integrated application environment, the PC-substrates can provide the noise suppression and spurious harmonic rejection needed for microwave components occupying close proximity [36, 37]. The PC-substrates can significantly reduce the number of filter stages that are essential to eliminate harmonics caused by amplification processes in all RF transmitters and receivers [38–40].

In this paper, we design and fabricate the bi-layered PC-substrate (of Fig. 1(b)), which consists of alternate dielectric materials. We present a systemic procedure to design PC-substrates based on the derivation of the effective dielectric constant. Such a systemic approach have not been presented in earlier works which are based mainly on simulation-based designs [34, 35]. Our analytical derivation of the effective permittivity is based on Microwave Bloch Analysis [41] in which infinite structures are assumed. The design is subsequently applied to the truncated practical structures. The fundamental band of the designed substrate is centered at 2 GHz and the bandgap lies between 4 to 5.5 GHz. We explain the formation of bandgaps and parameters such as the propagation constant and Bloch characteristic impedance by performing an exhaustive Bloch Analysis on the microstrip structure. Furthermore, a practical microwave device i.e., a 2.5 GHz coupled-line filter is designed to experimentally demonstrate the suppression of the second harmonic at 5 GHz. We anticipate that utilizing the photonic-crystal based substrates in an integrated multiband environment will eliminate the need of explicit filtering components, leading to dramatic size reduction of microwave devices [36].

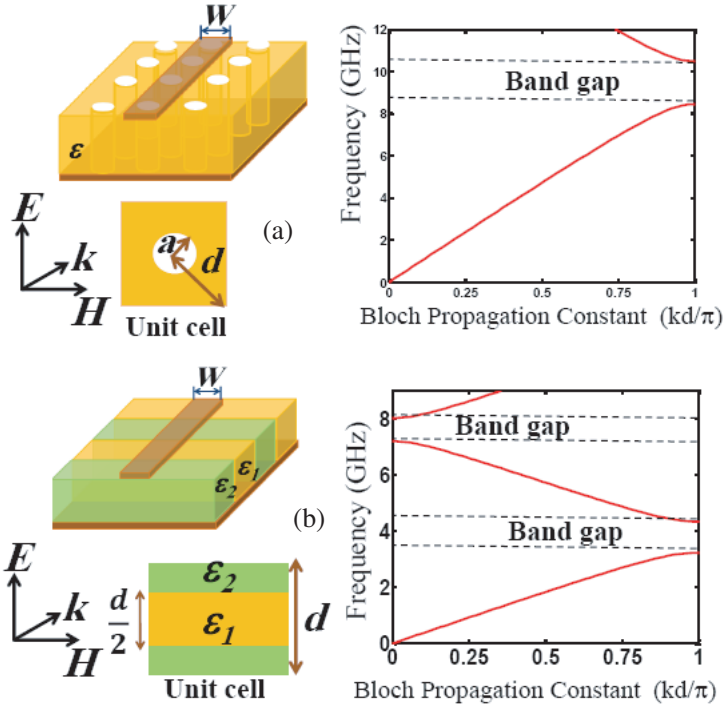

Figure 1. Photonic crystals used as substrates for microstrip structures (a) two dimensional photonic crystal designed with a background medium of $\varepsilon = 4$ by carving cylinders of radius $a = 0.25$ cm, repeated with periodicity of $d = 1$ cm. (b) One dimensional photonic crystal consists of alternating materials of high and low dielectric constants of $\varepsilon_1 = 2.3$ and $\varepsilon_1 = 6.15$ with a periodicity 'd' of 2 cm.

2. ANALYSIS OF THE BI-LAYERED PC-SUBSTRATE

The analysis includes two parts. First, the Bloch analysis which assumes infinite structures and involves the determination of the dispersion equation that governs the pass and stop bands and also leads to the determination of the effective permittivity. Second, the circuit analysis using the Kirchhoff's laws which is needed to calculate the transmission characteristics of the practical truncated structure. As shown in Fig. 1(a), the unit cell of the bi-layered photonic crystal can be drawn by assuming equivalent microstrip segments with substrate (relative) permittivities of ε_1 and ε_2 and characteristic impedances of Z_1 and Z_2. The effective intrinsic phase velocities (u_1, u_2) and the effective propagation constants (β_1, β_2) for the two types of microstrip transmission segments can be defined as:

$$u_1 = \frac{c}{\sqrt{\varepsilon_{e1}}}, \quad \beta_1 = \frac{\omega}{u_1}, \quad u_2 = \frac{c}{\sqrt{\varepsilon_{e2}}}, \quad \beta_2 = \frac{\omega}{u_2}. \tag{1}$$

ε_e is the effective relative permittivity of one of the photonic crystal layers and is related to the substrate's dielectric constant ε, height H and the strip width W by the following well-known equation [42]:

$$\varepsilon_e = \frac{\varepsilon + 1}{2} + \frac{\varepsilon - 1}{2} \frac{1}{\sqrt{1 + H/W}} \tag{2}$$

As depicted in Fig. 2(a), the unit cell is made symmetric by splitting the first line segment into two halves of length $d/4$ such that the periodicity (or the unit cell length) remains equal to d. The accumulative forward transmission ($ABCD$) matrix, which is the product of all the $ABCD$ matrices contributing to the unit cell, can then be defined as:

$$\begin{pmatrix} A & B \\ C & D \end{pmatrix} = \begin{pmatrix} \cos\theta_1 & jZ_1 \sin\theta_1 \\ \frac{j}{Z_1}\sin\theta_1 & \cos\theta_1 \end{pmatrix} \begin{pmatrix} \cos\theta_2 & jZ_2 \sin\theta_1 \\ \frac{1}{jZ_2}\sin\theta_1 & \cos\theta_2 \end{pmatrix} \begin{pmatrix} \cos\theta_1 & jZ_1 \sin\theta_1 \\ \frac{j}{Z_1}\sin\theta_1 & \cos\theta_1 \end{pmatrix} \tag{3}$$

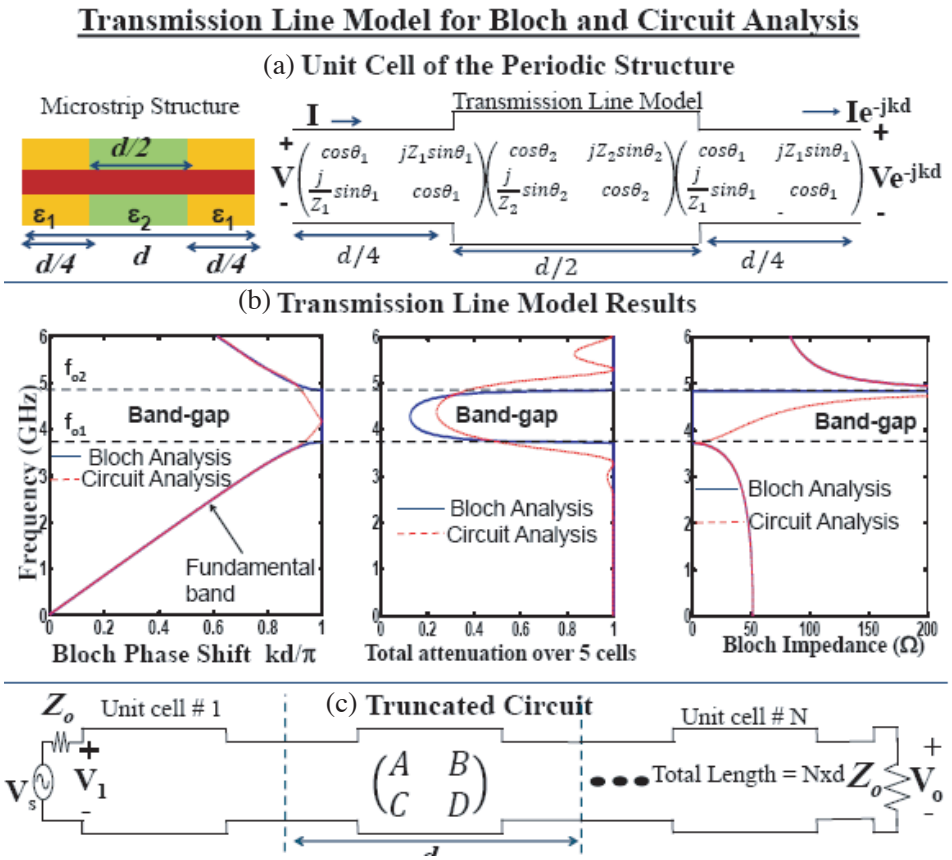

Figure 2. (a) Unit cell of the circuit model consists of a microstrip transmission line printed on a b-layered photonic crystal substrate comprising of alternate layers of materials of high and low dielectric constants. To maintain the symmetry, the unit cell length is d is divided into three segments. The forward transmission ($ABCD$) matrix is also shown for each microstrip segment. (b) The results of the Bloch analysis and truncated circuit analysis showing the phase and attenuation constants and the Boch impedance showing passbands and the bandgap. (c) Truncated circuit model of the periodic structure of (a).

where angles $\theta_1 = \beta_1 d/4$ and $\theta_2 = \beta_2 d/2$ define the intrinsic phase shifts incurred when an electromagnetic wave traverses over the two types of line segments. From the Bloch-Floquet Theorem, the circuit voltages and currents at the terminals can only differ by a phase of $e^{-\gamma d}$, where γ is the complex Bloch propagation constant of the periodic structure. Therefore, voltages and currents at the terminals of the unit cell are related by [42]:

$$\begin{pmatrix} A - e^{\gamma d} & B \\ C & D - e^{\gamma d} \end{pmatrix} \begin{pmatrix} Ve^{-\gamma d} \\ Ie^{-\gamma d} \end{pmatrix} = \begin{pmatrix} 0 \\ 0 \end{pmatrix}, \tag{4}$$

By applying the condition of non-trivial solution $(A - e^{\gamma d})(D - e^{\gamma d}) - BC = 0$ and the relation for symmetric circuits $AD - BC = 1$, the dispersion equation can be evaluated as:

$$\cosh \gamma d = \frac{A + D}{2}. \tag{5}$$

The Bloch impedance (Z_B) can be determined by finding the ratio of voltage and current at the output port of the unit cell (Fig. 2(a)),

$$Z_B = \frac{-B}{A - e^{\gamma d}}. \tag{6}$$

Consider the dispersion characteristics of the PC-based microstrip structure of Fig. 1(b). The real and imaginary parts of the Bloch propagation constant (6) are plotted in Fig. 2(b). Apart from a slight frequency shift, the Bloch propagation constant from the full-wave solver and the transmission line model look quite similar. The first bandgap extends from 3.75 GHz to 4.8 GHz. The peak in the imaginary part of the propagation constant signifies the attenuation in the band gap. Note that the Bloch impedance in the fundamental band is 50 Ω, which corresponds to the standard characteristic impedance of practical microwave devices.

Figure 2(b) also contains the calculated parameters for 5-unit-cell truncated microwave model, given in Fig. 2(c). The truncated model results are important because they show the circuit behavior in practical situations and also provide confidence to the designer. As observed, the infinite and truncated models behave close to each other when a reasonably long (10 cm) truncated periodic structure is considered. Note that the output voltage phase and attenuation characteristics (V_o/V_1) for the truncated model of N-unit-cells are calculated by applying Kirchhoff's current equations at the input and output nodes [43]:

$$\begin{pmatrix} V_1 \\ V_o \end{pmatrix} \begin{pmatrix} A & B \\ C & D \end{pmatrix}^N = \begin{pmatrix} V_s \\ 0 \end{pmatrix} \tag{7}$$

The characteristic impedance of the truncated structure (Z_{0m}) is calculated by first calculating the input impedances of the open and short circuited truncated structure (Z_{OC}, Z_{SC}) and using the relation:

$$Z_{0m} = \sqrt{Z_{OC} Z_{SC}} = \sqrt{\frac{A_t B_t}{C_t D_t}}. \tag{8}$$

where A_t, B_t, C_t, and D_t are the elements of the $ABCD$ matrix of the truncated model, given in Eq. (7). Finally, an important design parameter of a periodic structure is the effective dielectric constant which can be obtained by equating the Bloch propagation constant to the general phase relation:

$$kd = \frac{\omega \sqrt{\varepsilon_{eff}} d}{c}. \tag{9}$$

where k is the Bloch phase constant, and kd is the phase incurred over a unit cell and is obtained by taking the imaginary part of the dispersion relation in Eq. (5). For the design of the considered bi-layered PC-substrate, the effective dielectric constant at the center of the passband at around 2.5 GHz (see Fig. 2) is around 3.25.

3. EXPERIMENTAL RESULTS: HARMONIC SUPPRESSION

A practical 5-stage truncated microstrip structure using the bi-layered PC-substrate of periodicity (d) 2 cm is fabricated by alternatively placing 1 cm wide ×2 mm thick strips of Rogers RT/Duroid 5870 ($\varepsilon_r = 2.3$) and RO3006 ($\varepsilon_r = 6.15$) materials on a copper ground plane. The LPKF S62 CNC machine was used to precisely obtain the exact microstrip dimensions. The fabricated structure along with the experimental set-up to measure transmission coefficients with Anritsu MS2026 vector network analyzer (VNA) is depicted in Figs. 3(a)–(c). The measured transmission coefficient (S_{21}) along with the simulated results done using Agilent's ADS software are shown in Fig. 3(d). The stopband appears to be in the same approximate frequency band, as predicted in previous section using the infinite and truncated models of the structure. There is a slight shift of frequencies in the experimental results and an attenuation (of within 2 dB). The frequency shift between theory and experiment may be attributed to tolerance in the permittivity value of the Rogers substrate and the approximations assumed in the analytical microstrip rules that were used to calculate the amplitude response. The attenuation loss in the experimental transmission coefficient is due to the imperfections resulting from fabrication such as air gaps between the dielectric layers.

From Fig. 3(d), it can be observed that the measured stopband occurs approximately between 4 and 6 GHz. Hence if a microwave device that operates on a fundamental frequency between 2 and 3 GHz is designed, its second (spurious) harmonic would be suppressed. To demonstrate this effect, we design a 4-stage ($N = 3$) coupled-line bandpass filter centered at 2.5 GHz. The filter is designed following the standard 3rd order filter design procedure described in a microwave engineering textbook such as [42].

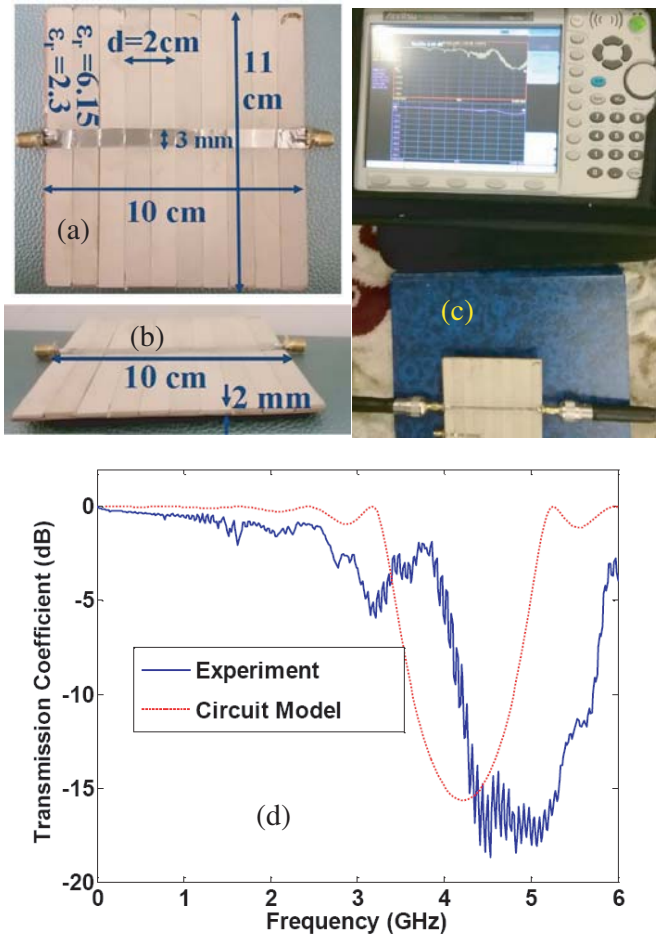

Figure 3. (a) Prototype of a 10 cm microstrip line printed on a photonic crystal substrate. The unit cell length is 2 cm and the dielectric layers consist of Rogers 5870 ($\epsilon_r = 2.3$) and RO3006 ($\epsilon_r = 6.15$). The effective relative permittivity of the substrate is 3.25. (b) Side view of the microstrip transmission line. (c) Measurement set-up with Anritsu MS2026 VNA. (d) Simulated and Measured transmission coefficient showing a bandgap between 4 GHz and 6 GHz.

Each stage consists of a coupled line of electrical length 90°. The even and odd impedances of the kth stage is given by the following equations [42]:

$$Z_{0e} = Z_0[1 + J_k Z_0 + (J_k Z_0^2)]Z_{0o} = Z_0[1 - J_k Z_0 + (J_k Z_0^2)], \tag{10}$$

where $J_k Z_0$ is different for each filter stage and is given in terms of the lowpass prototype values g_k and the fractional bandwidth Δ as follows:

$$J_1 = \sqrt{\frac{\pi\Delta}{2g_1}}, \quad J_2 = J_3 = \frac{\pi\Delta}{2\sqrt{g_2 g_2}}, \quad J_4 = \sqrt{\frac{\pi\Delta}{2g_3 g_4}}, \tag{11}$$

The dimensions of the equivalent microstrip coupled line sections corresponding to the even and odd impedances (10) can be obtained by using any standard Electromagnetic simulator program such as Agilent's ADS. The results of these calculations for a 3 dB equi-ripple filter designed on a substrate of effective dielectric constant 3.25 are summarized in Table 1, while Fig. 4(a) gives the graphical representation showing the widths (W) of the constituting transmission lines and the gaps (S) between them. The photograph of the filter prototype can be seen in the inset of Fig. 4(a). The VNA measurements of the transmission coefficient (S_{21}), given in Fig. 4(b), indeed demonstrate the suppression of the second harmonic that occurs at around 4.8 GHz. Fig. 4(b) also shows a simulation

Table 1. Design of a coupled-line maximally-flat band-pass filter using photonic-crystal based substrate.

n	g_k	$Z_0 J_k$	$Z_{0e}(\Omega)$	$Z_{0o}(\Omega)$	W (mm)	S (mm)
1	1	0.2166	63.17	41.51	3.2	0.65
2	2	0.1017	55.60	45.43	3.5	2.0
3	1	0.1017	55.60	45.43	3.5	2.0
4	1	0.2166	63.17	41.51	3.2	0.65

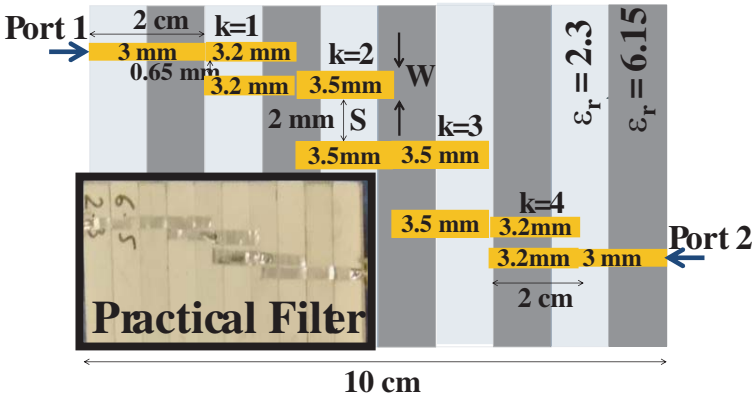

(a) Design of a 2.5 GHz Coupled Line 4-Stage Filter

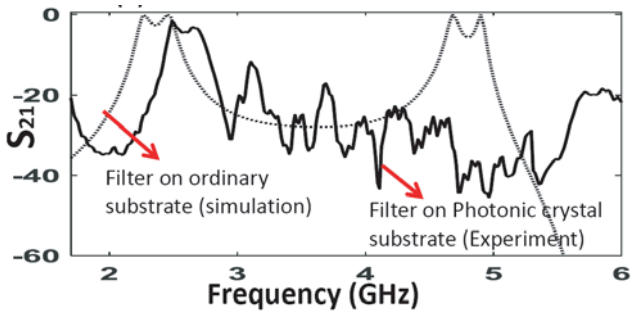

(b) Measurement and Simulation Results

Figure 4. (a) Design of 2.5 GHz coupled line 3 dB equi-ripple bandpass filter on the photonic crystal microwave substrate. The inset showing the practical implementation using Rogers materials with dielectric constants 2.3 and 6.15. (b) Transmission coefficient measured using VNA demonstrating the second harmonic suppression. Simulation results show the behavior of the conventional filter with the second harmonic appearing around 4.8 GHz.

of the a conventional coupled line filter designed on a substrate of $\varepsilon_r = 3.25$ showing a second passband at twice the fundamental frequency. The attenuation in the measured passband can be improved by employing better fabrication methods such as 3D printing.

4. CONCLUSION

We demonstrate the existence of *bandgaps* in microstrip lines fabricated on a substrate which is designed by using photonic crystals (*PC-substrate*). The substrate is designed by arranging an alternating pattern of high and low dielectric constants given by the values 6.15 and 2.3, respectively with a periodicity of 2 cm. We explain the dispersion properties of the structure by Boch analysis and plotting the resulting Brillouin diagram and the Bloch impedance plot. A practical microstrip structure

using the designed PC-substrate is constructed using commercially available dielectric materials from Rogers Corporation. A fundamental band and a bandgap centered at 2.5 GHz and a bandgap 4.5 GHz respectively experimentally shown. The suppression of second harmonic is practically demonstrated by designing a 3 dB equi-ripple coupled-line bandpass filter with a center frequency of 2.5 GHz. Measured transmission coefficient shows more than 30 dB suppression of the second harmonic at 5 GHz. The photonic crystals based substrate can be potentially applied in applications such as filtering and spurious harmonic suppression to free higher spectra that can be utilized for other devices located in close proximity. With three-dimensional printing becoming a common trend, we anticipate a broader scope of these engineered substrates.

REFERENCES

1. Yablonovitch, E., "Inhibited spontaneous emission in solid-state physics and electronics," *Physical Review Letters*, Vol. 58, No. 20, 2059, 1987.
2. John, S., "Strong localization of photons in certain disordered dielectric superlattices," *Physical Review Letters*, Vol. 58, No. 23, 2486, 1987.
3. Krauss, T. F., M. Richard, and S. Brand, "Two-dimensional photonic-bandgap structures operating at near-infrared wavelengths," *Nature*, Vol. 383, No. 6602, 699–702, 1996.
4. Meade, R., J. N. Winn, and J. Joannopoulos, *Photonic Crystals: Molding the Flow of Light*, 1995.
5. Datta, S., "Classical wave propagation in periodic and random media," Ph.D. Dissertation, Iowa State University, 1994.
6. Smith, D. R., W. J. Padilla, D. Vier, S. C. Nemat-Nasser, and S. Schultz, "Composite medium with simultaneously negative permeability and permittivity," *Physical Review Letters*, Vol. 84, No. 18, 4184, 2000.
7. Smith, D., J. Pendry, and M. Wiltshire, "Metamaterials and negative refractive index," *Science*, Vol. 305, No. 5685, 788–792, 2004.
8. West, P. R., S. Ishii, G. V. Naik, N. K. Emani, V. M. Shalaev, and A. Boltasseva, "Searching for better plasmonic materials," *Laser & Photonics Reviews*, Vol. 4, No. 6, 795–808, 2010.
9. Wang, Z., F. Cheng, T. Winsor, and Y. Liu, "Optical chiral metamaterials: A review of the fundamentals, fabrication methods and applications," *Nanotechnology*, Vol. 27, No. 41, 412001, 2016.
10. Shalaev, V. M., "Optical negative-index metamaterials," *Nature Photonics*, Vol. 1, No. 1, 41, 2007.
11. Engheta, N., "Circuits with light at nanoscales: Optical nanocircuits inspired by metamaterials," *Science*, Vol. 317, No. 5845, 1698–1702, 2007.
12. Gralak, B., S. Enoch, and G. Tayeb, "Anomalous refractive properties of photonic crystals," *JOSA A*, Vol. 17, No. 6, 1012–1020, 2000.
13. Notomi, M., "Negative refraction in photonic crystals," *Optical and Quantum Electronics*, Vol. 34, No. 1, 133–143, 2002.
14. Sievenpiper, D., L. Zhang, R. F. J. Broas, N. G. Alexopolous, and E. Yablonovitch, "High-impedance electromagnetic surfaces with a forbidden frequency band," *IEEE Transactions on Microwave Theory and Techniques*, Vol. 47, No. 11, 2059–2074, 1999.
15. Yang, F. and Y. Rahmat-Samii, *Electromagnetic Band Gap Structures in Antenna Engineering*, Cambridge University Press Cambridge, UK, 2009.
16. Eleftheriades, G. V. and K. G. Balmain, *Negative-refraction Metamaterials: Fundamental Principles and Applications*, John Wiley & Sons, 2005.
17. Verma, R. and K. Daya, "Effect of forbidden bands of electromagnetic bandgap engineered ground plane on the response of half wave length linear microwave resonator," *Journal of Applied Physics*, Vol. 109, No. 8, 084505, 2011.
18. Yang, L. M. Fan, F. Chen, J. She, and Z. Feng, "A novel compact electromagnetic-bandgap (EBG) structure and its applications for microwave circuits," *IEEE Transactions on Microwave Theory and Techniques*, Vol. 53, No. 1, 183–190, 2005.

19. Liang, J. and H. D. Yang, "Microstrip patch antennas on tunable electromagnetic band-gap substrates," *IEEE Transactions on Antennas and Propagation*, Vol. 57, No. 6, 1612–1617, 2009.
20. Laso, M., M. Erro, D. Benito, M. Garde, T. Lopetegi, F. Falcone, and M. Sorolla, "Analysis and design of 1-d photonic bandgap microstrip structures using a fiber grating model," *Microwave and Optical Technology Letters*, Vol. 22, No. 4, 223–226, 1999.
21. Gonzalo, R., P. De Maagt, and M. Sorolla, "Enhanced patch-antenna performance by suppressing surface waves using photonic-bandgap substrates," *IEEE transactions on Microwave Theory and Techniques*, Vol. 47, No. 11, 2131–2138, 1999.
22. Kelly, P. K., L. J. Diaz, M. J. Piket-May, and I. Rumsey, "Scan blindness mitigation using photonic bandgap structure in phased arrays," *Optical Devices and Methods for Microwave/Millimeter-Wave and Frontier Applications*, Vol. 3464, 239–248, International Society for Optics and Photonics, 1998.
23. Zhang, L., J. Castañeda, and N. G. Alexopoulos, "Scan blindness free phased array design using pbg materials," *IEEE Transactions on Antennas and Propagation*, Vol. 52, 2000–2007, 2004.
24. Da Silva, J. L., H. D. de Andrade, A. S. Maia, H. C. Fernandes, I. B. da Silva, A. S. Sombra, and J. P. Pereira, "Performance of microstrip patch antenna due EBG/PBG arrangements insertion," *Microwave and Optical Technology Letters*, Vol. 58, No. 12, 2933–2937, 2016.
25. Brown, E., C. Parker, and E. Yablonovitch, "Radiation properties of a planar antenna on a photonic-crystal substrate," *JOSA B*, Vol. 10, No. 2, 404–407, 1993.
26. Kazemi, H., J. Higgins, B. Herting, H. Xin, J. B. West, and J. Hacker, "Electromagnetic bandgap waveguide (EBG) phase shifters for low cost electronically scanned antennas (ESA)," *2007 IEEE Antennas and Propagation Society International Symposium*, 4357–4360, IEEE, 2007.
27. Hill, M. J., R. W. Ziolkowski, and J. Papapolymerou, "A high-Q reconfigurable planar EBG cavity resonator," *IEEE Microwave and Wireless Components Letters*, Vol. 11, No. 6, 255–257, 2001.
28. Jizat, N. M., Z. Yusoff, S. K. A. Rahim, M. I. Sabran, and M. T. Islam, "Exploitation of the electromagnetic band gap (EBG) in 3-dB multi-layer branch-line coupler," *2015 IEEE 12th Malaysia International Conference on Communications (MICC)*, 264–269, 2015.
29. Falcone, F., T. Lopetegi, and M. Sorolla, "1-d and 2-d photonic bandgap microstrip structures," *Microwave and Optical Technology Letters*, Vol. 22, No. 6, 411–412, 1999.
30. Goyal, A. K. and S. Pal, "Design analysis of bloch surface wave based sensor for haemoglobin concentration measurement," *Applied Nanoscience*, 2020.
31. Wang, R., H. Xia, D. Zhang, J. Chen, L. Zhu, Y. Wang, E. Yang, T. Zang, X. Wen, G. Zou, et al., "Bloch surface waves confined in one dimension with a single polymeric nanofibre," *Nature Communications*, Vol. 8, No. 1, 1–10, 2017.
32. Bashiri, J., B. Rezaei, J. Barvestani, and C. Zapata-Rodríguez, "Bloch surface waves engineering in one-dimensional photonic crystals with a chiral cap layer," *JOSA B*, Vol. 36, No. 8, 2106–2113, 2019.
33. "Mit photonic bands," https://mpb.readthedocs.io/en/latest/.
34. Qian, Y., V. Radisic, and T. Itoh, "Simulation and experiment of photonic band-gap structures for microstrip circuits," *Proceedings of 1997 Asia-Pacific Microwave Conference*, 585–588, IEEE, 1997.
35. Mbairi, F. and H. Hesselbom, "Microwave bandstop filters using novel artificial periodic substrate electromagnetic band gap structures," *IEEE Transactions on Components and Packaging Technologies*, Vol. 32, 273–282, July 2009.
36. Siddiqui, O. F. and A. S. S. Mohra, "A harmonic-suppressed microstrip antenna using a metamaterial-inspired compact shunt-capacitor loaded feedline," *Progress In Electromagnetics Research C*, Vol. 45, 151–162, 2013.
37. Ren, Y.-J., M. F. Farooqui, and K. Chang, "A compact dual-frequency rectifying antenna with high-orders harmonic-rejection," *IEEE Transactions on Antennas and Propagation*, Vol. 55, No. 7, 2110–2113, 2007.
38. Gyaang, R., D.-H. Lee, and J. Kim, "Analysis and design of harmonic rejection low noise amplifier with an embedded notch filter," *Electronics*, Vol. 9, No. 4, 596, 2020.

39. Chou, J.-H., D.-B. Lin, K.-L. Weng, and H.-J. Li, "All polarization receiving rectenna with harmonic rejection property for wireless power transmission," *IEEE Transactions on Antennas and Propagation*, Vol. 62, No. 10, 5242–5249, 2014.
40. Ma, Z. and G. A. Vandenbosch, "Wideband harmonic rejection filtenna for wireless power transfer," *IEEE Transactions on Antennas and Propagation*, Vol. 62, No. 1, 371–377, 2013.
41. Brillouin, L., "Wave propagation in periodic structures: Electric filters and crystal lattices," 1953.
42. Pozar, D., *Microwave Engineering*, 2nd Edition, John Wiley and Sons Inc., 1998.
43. Siddiqui, O. F., "The forward transmission matrix (FTM) method for S-parameter analysis of microwave circuits and their metamaterial counterparts," *Progress In Electromagnetics Research B*, Vol. 66, 123–141, 2016.